



Liquid antimony pentachloride as oxidant for robust oxidative chemical vapor deposition of Poly(3,4-ethylenedioxythiophene) films

Milad Mirabedin, Hugues Vergnes, Nicolas Caussé, Constantin Vahlas, Brigitte Caussat

► To cite this version:

Milad Mirabedin, Hugues Vergnes, Nicolas Caussé, Constantin Vahlas, Brigitte Caussat. Liquid antimony pentachloride as oxidant for robust oxidative chemical vapor deposition of Poly(3,4-ethylenedioxythiophene) films. *Applied Surface Science*, 2021, 554, pp.149501. 10.1016/j.apsusc.2021.149501 . hal-03188795

HAL Id: hal-03188795

<https://hal.science/hal-03188795>

Submitted on 2 Apr 2021

HAL is a multi-disciplinary open access archive for the deposit and dissemination of scientific research documents, whether they are published or not. The documents may come from teaching and research institutions in France or abroad, or from public or private research centers.

L'archive ouverte pluridisciplinaire **HAL**, est destinée au dépôt et à la diffusion de documents scientifiques de niveau recherche, publiés ou non, émanant des établissements d'enseignement et de recherche français ou étrangers, des laboratoires publics ou privés.








Open Archive Toulouse Archive Ouverte (OATAO)

OATAO is an open access repository that collects the work of Toulouse researchers and makes it freely available over the web where possible

This is an author's version published in: <http://oatao.univ-toulouse.fr/27679>

Official URL: <https://doi.org/10.1016/j.apsusc.2021.149501>

To cite this version:

Mirabedin, Milad  and Vergnes, Hugues  and Caussé, Nicolas  and Vahlas, Constantin  and Caussat, Brigitte  *Liquid antimony pentachloride as oxidant for robust oxidative chemical vapor deposition of Poly(3,4-ethylenedioxythiophene) films.* (2021) Applied Surface Science, 554. 149501. ISSN 0169-4332

Any correspondence concerning this service should be sent to the repository administrator: tech-oatao@listes-diff.inp-toulouse.fr

Liquid antimony pentachloride as oxidant for robust oxidative chemical vapor deposition of poly(3,4-ethylenedioxythiophene) films

Milad Mirabedin^{a,b}, Hugues Vergnes^a, Nicolas Caussé^b, Constantin Vahlas^b, Brigitte Caussat^{a,*}

^a *Laboratoire de Génie Chimique, Université de Toulouse, CNRS, 4 allée Emile Monso, 31030 Toulouse Cedex 4, France*

^b *CIRIMAT, Université de Toulouse, CNRS, 4 allée Emile Monso, 31030 Toulouse cedex 4, France*

ARTICLE INFO

Keywords:

Oxidative chemical vapor deposition
Conductive polymers
PEDOT
Thin films
EDOT
SbCl₅

ABSTRACT

The oxidative chemical vapor deposition (oCVD) process is investigated to produce poly (3,4-ethylenedioxythiophene) (PEDOT) thin films on 10 cm diameter Si wafers, involving the SbCl₅ liquid oxidant. Process/structure/properties correlations are thoroughly studied, including the influence of the SbCl₅/EDOT ratio, substrate temperature (T_{sub}), total pressure and deposition duration, on the thickness, composition, morphology, spatial uniformity of the films, and on their electrical conductivity and optical transmittance. The electrical conductivity of the films increases by decreasing the oxidant/EDOT ratio and by increasing the substrate temperature. Such increase of substrate temperature results in the decrease of the deposited mass and thickness. Films uniformity and electrical conductivity are improved by decreasing the total pressure. Operating at 75 Pa results in films of equal and uniform thickness deposited on substrates located all over the deposition chamber, proving the potential of the PEDOT-SbCl₅ oCVD process to be scaled up over larger surfaces. The absence of post deposition liquid rinsing allows developing a full dry process, which is of interest to coat sensitive substrates and can thus be implemented for the processing of devices requiring durable, transparent, conductive PEDOT thin films, in particular in the field of optoelectronics.

1. Introduction

The growing development of electronic and optoelectronic devices such as organic light-emitting diodes (OLEDs) and organic solar cells require scalable and transparent electrodes, composed of thin films that simultaneously provide electrical conductivity, flexibility and optical transparency [1–3]. Conducting polymers present unique advantages over more common inorganic materials, namely cost effectiveness, lightweight and resource abundance, while ensuring satisfactory electrical conductivity. They can be conveniently processed, even on flexible substrates [3]. Nowadays, they are considered as “a new generation of materials which exhibit the electrical properties of metals or semiconductors and retain the attractive mechanical properties and processing advantages of polymers” [4]. Poly(3,4 ethylenedioxythiophene) (PEDOT) is among the most chemically and thermally stable conducting polymers. It is commercialized in its dispersion form mixed with polystyrene sulfonate (PSS) polymer [5]. Thin films of PEDOT:PSS are most often processed by spin coating from aqueous mixtures of PSS and PEDOT and are now present in OLEDs, supercapacitors, solar cells, electrochromic devices and other devices [6].

Since two decades, vapor phase deposition processes, in particular vapor phase polymerization (VPP) [7] and oxidative chemical vapor deposition (oCVD) [8] have been developed to avoid the substrate-solvent incompatibility of liquid solution technologies and to provide conformal coatings on complex porous substrates. In VPP and oCVD, the oxidant serves both to promote monomer polymerization and to subsequently oxidize the neutral polymer to form the conductive, doped polymer. According to Lock et al. [8], the formation of PEDOT follows a Step Growth Polymerization (SGP) mechanism, requiring the simultaneous presence of monomer and oxidant for continuous polymerization. VPP still involves a first liquid step to deposit the oxidant layer, followed by the introduction of EDOT vapors at a second step. The polymerization stops when the oxidant is no more available, even if EDOT vapor is still present [9]. In contrast, oCVD is a one-step purely gas phase technique, allowing to control the film thickness by varying the deposition time. Provided the vaporized oxidant flow rate is fully controlled, it yields films whose characteristics and properties can be finely tuned.

The nature of the oxidant plays an important role in the characteristics of oCVD PEDOT films [9,10]. Oxidants are mostly ionic compounds with one of their atoms belonging to the halogen group, mainly

* Corresponding author.

E-mail address: brigitte.caussat@ensiacet.fr (B. Caussat).

chosen for their oxidation potential. Common drawbacks are their sensitivity to oxygen and humidity, their corrosive nature and their toxicity. Since the introduction of oCVD of PEDOT by Gleason and co-workers [8], several solid oxidants have been used to produce PEDOT films from EDOT monomer. Among them, iron trichloride (FeCl_3) is the most studied one [8,11–14], because of its availability and relatively low toxicity [15,16]. However, sublimation of solid oxidants is challenging as these compounds are highly hygroscopic and require manipulation under inert atmosphere [17]. In a previous study, we demonstrated that the sublimation of FeCl_3 in a conventional crucible was only active for the first minutes of process, due to unavoidable oxidation and sintering of the powder and we concluded that the stability of the sublimation rate over time is a prerequisite for process implementation [11]. Besides this process issue, FeCl_3 derivatives and residues are often present in oCVD processed PEDOT films due to oxidant condensation during deposition. These hygroscopic contaminants degrade the electrical conductivity and the durability of the films, and require additional steps of post deposition liquid rinsing to remove them [18].

For these reasons, solid oxidants have been progressively replaced by easier to vaporize liquid ones, such as bromine (Br_2) [19], and more recently sulfuric acid (H_2SO_4) [20], molybdenum(V) chloride (MoCl_5) [21], vanadium oxytrichloride (VOCl_3) [22–24] and antimony(V) pentachloride (SbCl_5) [24,25]. SbCl_5 appears to be cost effective and among the less toxic compounds of this list. To the best of our knowledge, the only works available on oCVD of PEDOT from SbCl_5 are that of Kaviani et al. [24] and of Gharahcheshmeh et al. [25]. The latter recently studied the correlations existing between nanostructure, crystal state and electrical conductivity of PEDOT thin films, in order to optimize their optoelectronic properties. They succeeded in reaching significantly high electrical conductivities up to 7500 S/cm, by operating at 140 °C deposition temperature and in the presence of water vapor. Water vapor appears to facilitate the PEDOT linear polymerization forming the conductive quinoid structure, by exalting the oxidant SbCl_5 decomposition into Cl^- dopant. Kaviani et al. [24] investigated the electrocatalytic activity in oxygen reduction reaction of PEDOT films deposited on carbon substrates without, however, correlating the films characteristics with the deposition conditions. This is the focus of the present work, with an ultimate objective to develop a robust one-step full dry oCVD process for the production of PEDOT thin films of controlled characteristics and properties.

We first study the stability over time of the vaporized SbCl_5 oxidant flow rate to guarantee a full control of the process, in particular of the film thickness. Then, we analyze the influence of the SbCl_5 /EDOT molar ratio, substrate temperature, total pressure and deposition duration on the mass, thickness, uniformity, morphology, chemical composition,

and electrical conductivity of the films, without any post deposition rinsing step. We finally investigate in details the film uniformity over a large scale inside the reactor chamber.

2. Materials and methods

oCVD experiments are performed in a custom-built stainless steel reactor (Mageva, Neyco®), as illustrated in Fig. 1a and already presented in [11]. The reactor (total effective volume of 17 l) is equipped in its top part with a ceramic substrate holder heated by Joule effect fixed horizontally at the lid. A thermocouple is placed over the back of the ceramic and is connected to a PID controller to monitor the substrate temperature (T_{sub}) between 25 and 130 °C with an accuracy of 0.8%. The total pressure is controlled within the range 1–133 Pa by a system composed of a Leybold Ruta 501 pump, a gate valve and a Baratron pressure gauge. Unless otherwise mentioned, the total pressure is fixed at 75 Pa and the deposition time is kept at 30 min.

PEDOT films were produced from monomeric 3,4-ethylenedioxythiophene (EDOT, 97%, Sigma-Aldrich) and SbCl_5 (99%, Acros Organic). The liquid SbCl_5 was evaporated from a bubbler immersed in a thermally-regulated bath at 90 °C. At this temperature, the SbCl_5 saturation vapor pressure is close to 5000 Pa [26]. The bubbler was loaded in a glove box under argon atmosphere. The flow rate of the SbCl_5 vapors was adjusted with a needle valve placed on the gas line at the exit of the bubbler. EDOT was vaporized in another bubbler, also immersed in a thermally-regulated bath in the range 65–90 °C. The EDOT saturation vapor pressure at 90 °C is 1000 Pa. All gas lines between the bubblers and the reactor inlets were heated at 100 °C to avoid condensation. 10 standard centimeters per minute (sccm) of nitrogen (99.999%, Air Liquide) were also sent into the reactor during the depositions. PEDOT films were deposited on 10 cm Si (100) wafers, used as received. Their sheet resistance was measured as close to $35 \pm 5 \text{ k}\Omega/\square$, significantly high to avoid sheet resistance correction due to parallel conduction of the substrate. No post deposition treatment was applied.

Before and after each experiment, the mass difference of the SbCl_5 bubbler, of the EDOT jar and of the silicon wafer was systematically determined using a KERN ABS 320-4 N balance with a precision of 0.1 mg for the two bubblers, and a Sartorius R180D balance with a precision of 0.01 mg for the substrate. This procedure allowed to ascertain the flow rates of the vaporized EDOT and SbCl_5 , thus the inlet molar SbCl_5 /EDOT ratio, and the mass of the deposited film.

Film thickness was measured by profilometry with a DektakXT instrument with a 2 μm stylus tip radius and 3 mg stylus load. Measurements were performed on consecutive 1 cm distant points, along two perpendicular x and y diameters. Step heights were made on purpose by

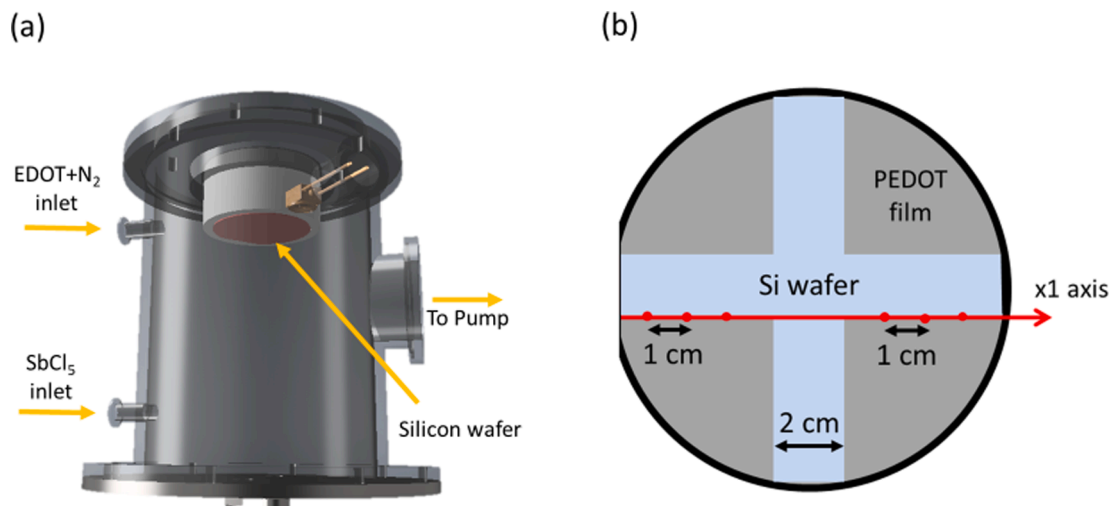


Fig. 1. Schematic view of (a) the oCVD reactor, (b) the substrate with the cross in Kapton tape.

covering prior deposition a 2 cm large cross-zone of the substrates with a Kapton tape (Fig. 1 b), allowing a $56 \pm 3 \text{ cm}^2$ deposition surface on the Si wafer. Three measurements were made at each position and then averaged. Scanning electron microscopy (SEM) (Helios NanoLab 600i) was used to check the film thickness on cross-sections of selected samples cut in liquid nitrogen and to investigate the surface morphology on top view micrographs.

Atomic Force Microscopy (AFM) maps were obtained using an Agilent Technologies AFM/STM 5500 (PicoPlus) microscope. Film composition was analyzed using transmission Fourier transform infrared spectrometry (FTIR), performed in a PerkinElmer Spotlight 400 bench with 16 scans at 4 cm^{-1} resolution. Optical transmittance of films deposited on purpose on glass substrates (Deckglaser 0101062) was measured using an Agilent Cary 5000 UV-Vis spectrometer within the range 300–800 nm. A scan rate of 600 nm/min with 2 nm spectral band width (SBW) was applied. The film sheet resistance R_s (Ω/\square) was measured on the wafer substrates with a Signatone S-302-4 four-point probe station. A constant current of 200 nA was applied with a Keithley 6220 instrument, and the corresponding voltage was read on a Keithley 2182A one. The electrical conductivity σ (S/cm) was deduced from Eq. (1) where t is the thickness of the film (cm) [27].

$$\sigma = \frac{1}{R_s t} \quad (1)$$

3. Results and discussion

3.1. Preliminary study on the oxidant flow rate stability

Continuous and constant presence of oxidant vapor is mandatory to produce in a controlled way PEDOT films by oCVD, as explained in introduction. With the aim to probe the evaporation rate of SbCl_5 , we monitored the weight loss of the SbCl_5 bubbler for 3 evaporation durations, 30, 60 and 120 min in the conditions of PEDOT deposition experiments, i.e. at a total pressure of 75 Pa under 10 sccm of N_2 . The results are reported in Fig. 2. The evaporated mass of SbCl_5 linearly increases from 134 to 551 mg when the evaporation time is increased from 30 min to 120 min, providing a constant flow rate of 4.5 mg/min (or 0.35 sccm) of gaseous SbCl_5 . It is concluded that SbCl_5 can be vaporized in a continuous mode, thus offering the possibility to fully control the oCVD process.

It is important to note that due to the high saturation pressure of SbCl_5 vapors (150 Pa at 20°C) in comparison to its partial pressure in the reactor (close to 2.5 Pa), we did not observe any droplets of condensed SbCl_5 forming on the reactor walls or on a Si wafer intentionally placed for this purpose on the substrate holder, even at ambient temperature.

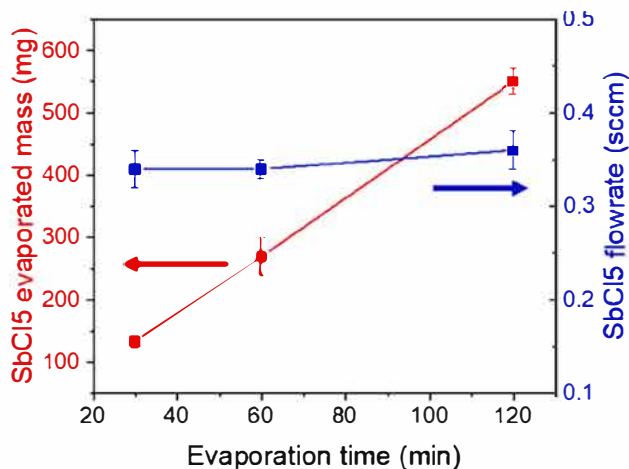


Fig. 2. Evolution of the SbCl_5 evaporated mass versus evaporation time.

This is an advantage of the SbCl_5 involving oCVD process in comparison with FeCl_3 , since the cleaning procedure of the reactor between two deposition experiments is simplified.

3.2. Influence of the inlet $\text{SbCl}_5/\text{EDOT}$ molar ratio

With the aim to investigate the influence of the composition of the input gas on the films characteristics and on their electrical conductivity we performed a series of depositions at 25°C fixed T_{sub} and at different inlet $\text{SbCl}_5/\text{EDOT}$ molar ratios in the range 0.18 to 3.00. For the ratios between 0.18 and 0.76, the EDOT flow rate was varied between 2.1 and 0.85 sccm for a constant SbCl_5 flow rate of 0.26 sccm. For the $\text{SbCl}_5/\text{EDOT}$ ratios of 2.08 and 3.00, the EDOT flow rate was kept constant at 0.42 sccm and the SbCl_5 flow rate was varied between 0.86 and 1.26 sccm. In all runs, the total gas flow rate ($\text{EDOT} + \text{SbCl}_5 + \text{N}_2$) was kept constant at 10–11 sccm; i.e. close to the N_2 flow rate, except for the run with the lowest $\text{SbCl}_5/\text{EDOT}$ ratio of 0.18 where, due to the high EDOT flow rate, the total gas flow slightly increased to 12.5 sccm.

Fig. 3a details the evolution of the mass and average thickness of the deposited films. It appears that when the $\text{SbCl}_5/\text{EDOT}$ ratio increases from 0.18 to 0.76 corresponding to the decrease of EDOT flow rate, the mass of the film slightly increases whereas its thickness slightly decreases. This opposite variation could be due to an evolution of the film porosity, since the FTIR results detailed later do not show any $-\text{OH}$ peak indicating the absence of hydrophilic by-products related to possible antimony oxides. The weak mass evolution indicates that in this process window, the EDOT supply is not a markedly limiting factor of the process. For ratios higher than 0.76 corresponding to increasing SbCl_5 flow rates, both the mass and thickness of the film sharply increase. This result clearly demonstrates that for these conditions, the deposition of

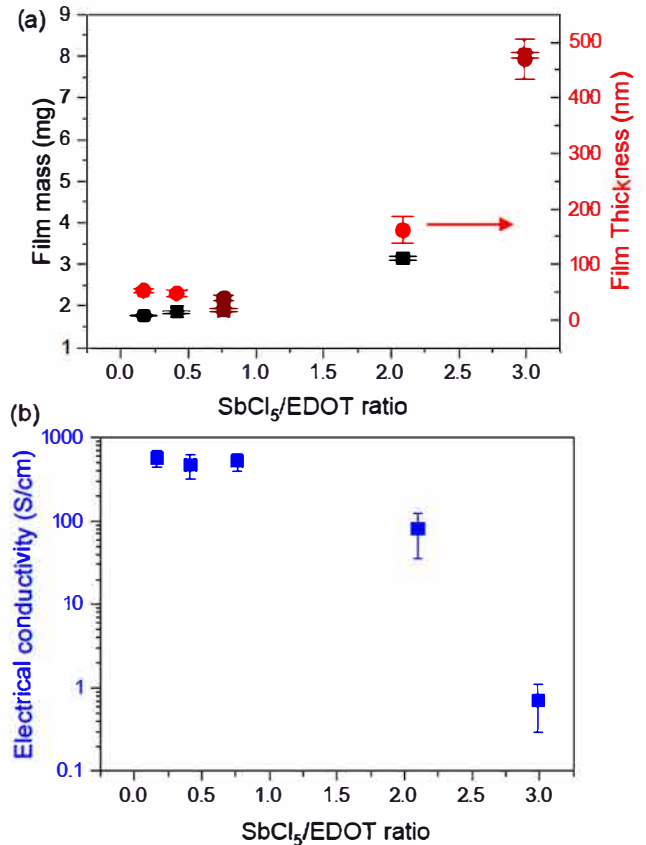


Fig. 3. (a) Average film thickness and mass and (b): Electrical conductivity as a function of the $\text{SbCl}_5/\text{EDOT}$ ratio (T_{sub} of 25°C , total pressure of 75 Pa and deposition duration of 30 min).

PEDOT is controlled by the SbCl_5 flow rate, as observed with other oxidants in particular FeCl_3 [11]. The deposition rate varies from 0.059 mg/min (1.8 nm/min) to 0.268 mg/min (15 nm/min), for SbCl_5 /EDOT ratios 0.18 and 3.00, respectively. These values are higher than the only deposition rates values available in the literature for PEDOT oCVD from SbCl_5 [25], which are between 0.45 and 3.75 nm/min, probably because of the lower total pressure (20 Pa) and higher substrate temperature these authors used.

The electrical conductivity of the films is presented in Fig. 3b as a function of the SbCl_5 /EDOT ratio. It remains in the same range of values (470–570 S/cm) when decreasing the EDOT flow rate, for SbCl_5 /EDOT ratios between 0.18 and 0.76. The highest conductivity obtained at ambient temperature in the present series of experiments without any post deposition treatment is 571 S/cm, which is higher than the conductivities obtained for PEDOT- SbCl_5 films at 100 °C after post deposition acid rinsing [24], but much lower than the values obtained at 140 °C using water vapor [25]. The PEDOT- SbCl_5 conductivities are generally higher than those of the PEDOT- FeCl_3 films deposited at ambient temperature [11]. The conductivity is much lower, below 100 S/cm, for higher SbCl_5 /EDOT ratios of 2.08 and 3, corresponding to the higher SbCl_5 flow rates tested. Let us note that for the conditions tested, the film thickness has no noticeable impact on the electrical conductivity, as will be detailed later. The overall decrease of the electrical conductivity with increasing the oxidant/EDOT ratio is in agreement with previous observations on oCVD PEDOT films from SbCl_5 [25], FeCl_3 [11] and VOCl_3 [23]. Since the conductivity of the film deposited at a SbCl_5 /EDOT ratio of 3 is close to 0, we did not consider this sample in the following sections.

The profiles of the film thickness over the 10 cm Si wafer are shown in Fig. 4 along the x1 axis (described in Fig. 1b) for the samples deposited with SbCl_5 /EDOT ratios 0.18 and 2.08. The average thickness of the film processed at a 0.18 ratio is constant along the wafer diameter, at 50 ± 5 nm. A similar behavior was observed for films processed with SbCl_5 /EDOT ratios as high as 0.76. The average thickness of the film processed with a ratio of 2.08 is significantly higher with a mean value of 480 nm and a strong deviation of ± 60 nm, probably due to the higher roughness of the film, as detailed below.

Fig. 5a presents FEG SEM surface micrographs of the films deposited with SbCl_5 /EDOT ratios 0.18, 0.42, 0.76 and 2.08. Low magnification micrographs reveal two different zones, namely a dark continuous surface covered by bright particles. The high magnification micrograph of the film deposited at a SbCl_5 /EDOT ratio 0.18 presents three zones: large bright regions over the surface, which are encountered with small bright particles all over a rough dark background. The small particles and dark

background are present in other samples as well, but for the highest SbCl_5 /EDOT ratio analyzed (2.08), the large bright regions are replaced by larger particles of hundred nanometers in diameter.

AFM maps of several samples (Fig. 5b) show that the bright particles or islands are significantly thicker than the underneath film. At a SbCl_5 /EDOT ratio 0.18, their height reaches 80 nm and increases to 180 nm and 400 nm for the ratios 0.42 and 0.76, respectively, all on a $10 \times 10 \mu\text{m}^2$ zone. These islands were not visible by profilometry, probably due to the pressure applied on the polymeric film by the stylus, which could crush them.

EDX and Raman analysis of these samples (Figures S1, S2 and S3 and Table S1 of Supplementary Materials) reveal all PEDOT signatures on the entire surface of the films, including the particles. According to localized Raman probing, the bright particles contain less quinoid (doped) PEDOT in comparison with the other zones and are consequently less conductive. This could explain the decrease of conductivity for the roughest films produced at the highest SbCl_5 flow rates tested.

Sb was equally detected by EDX and XPS all over the surface of the films (Figures S1 and S4 and Table S2 of Supplementary Materials), at an average concentration not exceeding 5 at.%, in agreement with recently published results [25]. The presence of Sb may be due to the formation of Sb-complexes on the PEDOT film through polymerization and reduction of adsorbed SbCl_5 after losing two chlorine atoms. SbCl_3 is indeed the most common oxidant by-product of SbCl_5 decomposition [25]. Based on this assumption, the formation of bonds between SbCl_3 and the oxygen in monomer ethylenedioxy rings results in trapping Sb during the film growth, as proposed by Kaviani et al. [24] for PEDOT films containing comparable amounts of Sb. The concentration of Sb in the films is lower than that of Fe in PEDOT films deposited from FeCl_3 [11]. This difference can be attributed to the fact that, in contrast to FeCl_3 , gaseous SbCl_5 cannot condensate on the film surface in the adopted operating conditions.

Fig. 6a presents FTIR spectra of the films processed with SbCl_5 /EDOT ratios between 0.18, 0.42, 0.76 and 2.08. Their intensity is normalized to that of the C-O-C stretching bond at 1091 cm^{-1} , since the corresponding peak is not modified by polymerization. Table S3 in Supplementary Materials details the attribution to the different bond vibrations of all peaks in the $2000\text{--}400 \text{ cm}^{-1}$ range. All PEDOT peaks are observed in all samples and no peak is observed in this range corresponding to SbCl_5 and its byproducts. No OH peak is observed at 3400 cm^{-1} meaning that PEDOT- SbCl_5 films are not contaminated by humidity. This is differentiating advantage compared to PEDOT- FeCl_3 films [11].

The normalization of the spectra with regard to the C-O-C stretching peak at 1091 cm^{-1} allows comparing the C-C antisymmetric stretching peak at 1527 cm^{-1} . It is known that the intensity of the C-C peak increases with the conjugation length of PEDOT [13] and that such an increase enhances the electrical conductivity of conductive polymers [28]. The histogram of Fig. 5b shows that the under peak area of the C-C peak decreases with increasing the SbCl_5 /EDOT ratio, which is in agreement with the conductivity results of Fig. 3b.

The results presented in this section allow concluding that the most conductive PEDOT films formed at 25 °C are the most uniform and smoothest ones, deposited with the lowest SbCl_5 (0.35 sccm) and the highest EDOT (2 sccm) flow rates tested, corresponding to an inlet SbCl_5 /EDOT molar ratio of 0.18.

3.3. Influence of the substrate temperature

Convergent literature information [8,16,29] concludes on the improvement of the conductivity when T_{sub} is increased, due to the reorganization of the conjugation in the backbone of the polymer. In the present section, we investigate the influence of T_{sub} in the range 25–70 °C, for the lowest SbCl_5 /EDOT ratio tested in the previous section (0.18).

Fig. 7a details the evolution of the film thickness and mass as a function of the inverse T_{sub} . It is recalled that all runs were performed

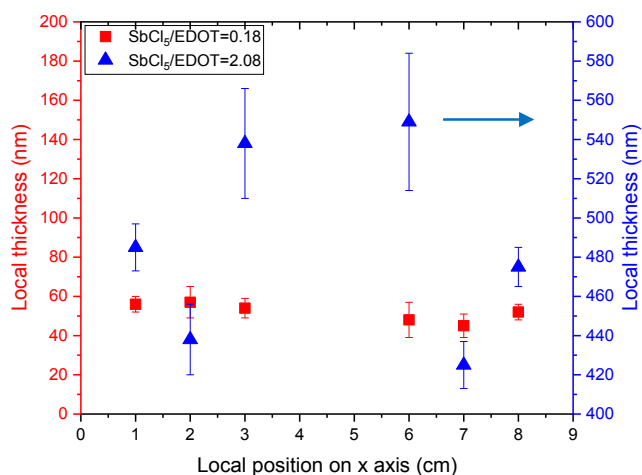


Fig. 4. Thickness profiles along the x1 axis for films deposited with inlet molar SbCl_5 /EDOT ratios of 0.18 and 2.08 (T_{sub} of 25 °C, total pressure of 75 Pa and deposition duration of 30 min). Note the same scale for the two ordinates.

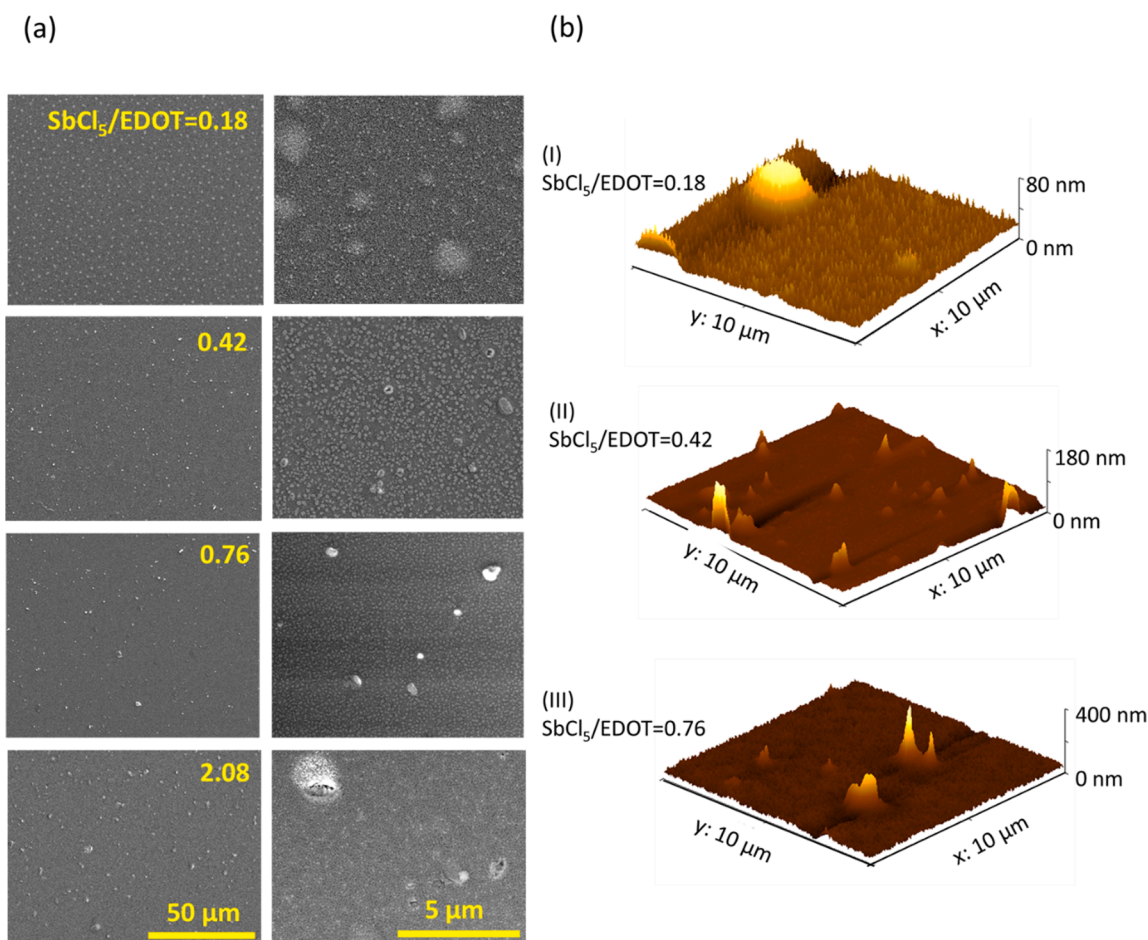


Fig. 5. (a) Surface FEG SEM micrographs and (b) AFM views of films deposited with different $\text{SbCl}_5/\text{EDOT}$ ratios (T_{sub} of 25 °C, total pressure of 75 Pa and deposition duration of 30 min).

during 30 min. The increase of T_{sub} from 25 to 50 °C results in the decrease of both the mass and the thickness, from 1.78 to 0.08 mg and from 54 nm to 12 nm, respectively. The deposition rate decreases from 0.059 mg/min to 0.003 mg/min. Operating at 70 °C did not result in film formation, verified by sample weighting, profilometry and FTIR. This influence of T_{sub} on the mass and thickness of the film is in agreement with recent results obtained at 90 and 140 °C [25]. It is however opposite to what we observed during a previous study with FeCl_3 [11]. Considering that the SbCl_5 flow rate is the limiting factor of the oCVD process in the conditions tested as previously demonstrated, this behavior may be due to the low and decreasing SbCl_5 concentration existing near the heated substrate with increasing T_{sub} . This is in agreement with the results of Li et al. [30] who found for the oCVD of PANI from aniline and SbCl_5 that the process is most likely limited by reactant adsorption on the substrate surface because higher temperatures generally reduce vapor-to-surface adsorption (or sticking coefficient) and, therefore, reduce the amount of reactant at a surface available for reaction. T_{sub} has no clear influence on the film uniformity as shown in Figure S5 of Supplementary Materials.

The results presented in Fig. 7b reveal that the electrical conductivity slightly increases from 571 to 770 S/cm with increasing T_{sub} . The most conductive film is obtained at the highest T_{sub} tested allowing the formation of the film (50 °C) [11]. We confirm the positive impact of T_{sub} on the electrical conductivity of oCVD PEDOT, as found elsewhere [16,25,29,31–32]. The conductivity of 770 S/cm at T_{sub} at 50 °C is slightly higher than that of Kaviani et al. [24] at 120 °C (701 S/cm) for oCVD of PEDOT from SbCl_5 . Even if this article does not detail all the deposition parameters, this may be due to the use of smaller $\text{SbCl}_5/\text{EDOT}$

EDOT ratios in the present work (0.18 vs. 3 in [24]). This behavior could be attributed to the lower deposition rate, allowing a possible organization of the polymer chain in a way that could increase the conjugation length and improve the conductivity. The maximum conductivity we obtained is however much lower than the recent one of Gharahcheshmeh et al. [25], confirming their statement that process parameters profoundly affect the texture and nanostructure of oCVD PEDOT thin films. A lower total pressure (20 Pa), a higher T_{sub} (140 °C) and the addition of water vapor probably explain this improvement.

Fig. 8 presents FEG SEM surface micrographs of films deposited at 25 and 50 °C. Increasing T_{sub} leads to a size reduction of the large bright islands. The highest magnification views show that the surface morphology is modified by increasing T_{sub} through the formation of nodules whose size is ca. 50 nm. Raman analysis (Figure S6) revealed that both the bright islands and the zones with smaller particles in SEM images for films deposited at 50 °C contain quinoid PEDOT, which is coherent with the fact that the film morphology evolution is not detrimental to the conductivity.

The normalized FTIR spectra are presented in Fig. 9a for the samples with T_{sub} equal to 25, 35 and 50 °C. All the peaks are associated to those of PEDOT. Again, no OH peak was observed at 3400 cm^{-1} . The intensity of the C–C stretching peak at 1527 cm^{-1} slightly increases with T_{sub} for these normalized transmittance spectra, as presented in Fig. 9b. As can be seen, the under curve area slightly increases with T_{sub} , in agreement with the electrical conductivity evolution (Fig. 7b).

XRD analysis revealed that the films do not diffract X-rays, even for the highest T_{sub} tested (Figure S7 in Supplementary Material), in agreement with the results of Kaviani et al. [24].

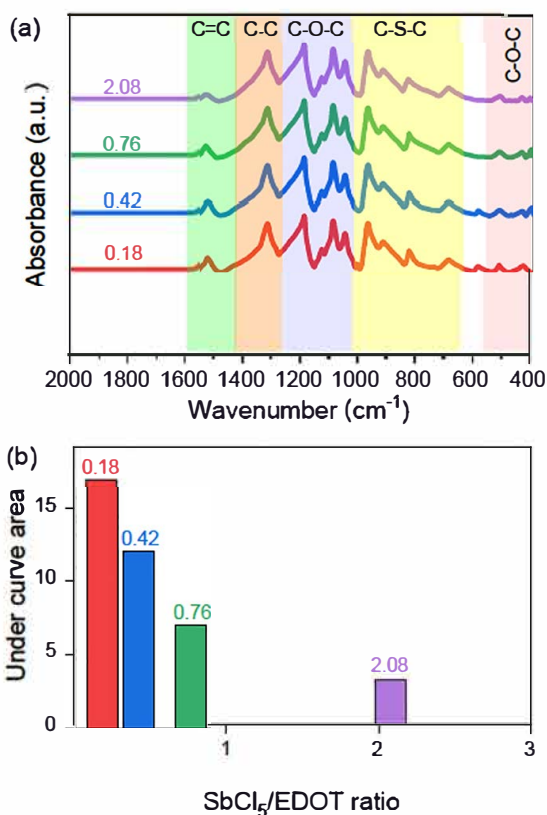


Fig. 6. (a): FTIR spectra obtained for the films with different SbCl₅/EDOT ratios, (b): Under curve areas of the corresponding C = C peak (1527 cm⁻¹).

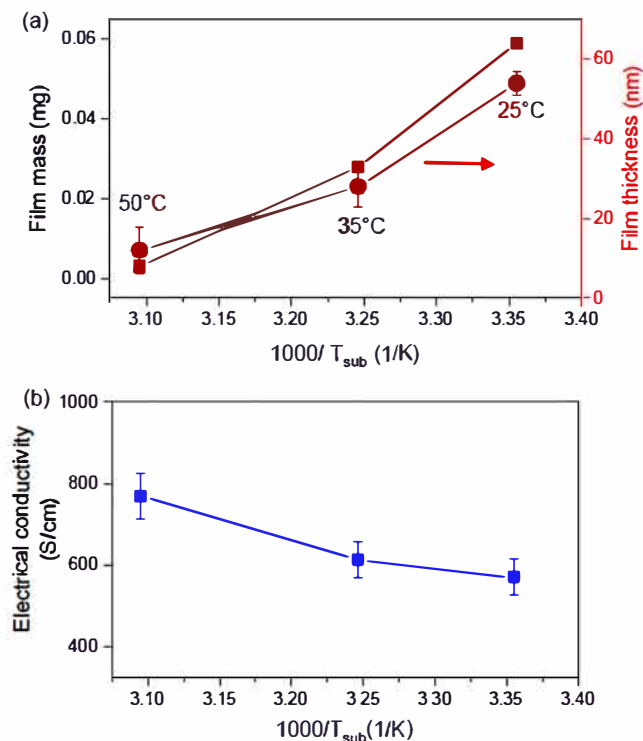


Fig. 7. Evolution of (a) the film thickness and mass, (b) the electrical conductivity versus 1000/T_{sub} (total pressure of 75 Pa, SbCl₅/EDOT ratio of 0.18 and deposition duration of 30 min).

3.4. Influence of the total pressure

The concentration of the gas species increases with the total pressure, which may result in higher deposition rates. In order to probe this trend, two deposition experiments were performed at T_{sub} 50 °C, SbCl₅/EDOT ratio 0.18 and two total pressures, 75 and 135 Pa. The obtained results are resumed in Table 1. As can be seen, the deposited mass increases from 0.08 to 3.46 mg and the average thickness increases from 12 to 287 nm when the pressure is increased. A less than twofold increase of the pressure then leads to a 43 fold increase of the mass of the films while at the same time, the electrical conductivity decreases by 30% from 770 ± 56 S/cm to 537 ± 116 S/cm.

It is worth noting that deposition at 135 Pa results in a strong decrease of films uniformity (Figure S8 of Supplementary Materials). The film thickness at 75 Pa is 12 ± 4 nm, while a thickness profile varying between 120 nm and 600 nm is observed at 135 Pa. The higher deposition rate is attributed to the increased reactants concentration at higher total pressure, while the simultaneously observed thickness non-uniformity could be due to a higher roughness of the film, as observed in Section 3.2 for the highest flow rates of SbCl₅ tested.

The normalized FTIR spectra are presented in Fig. 10a for the two samples. All the peaks are associated to those of PEDOT. In addition, an OH peak at 3350 cm⁻¹ is present for the film at 135 Pa (not shown), probably due to an excess of hydrophilic by-products related to the higher SbCl₅ concentration, since the characterization was performed under ambient air. Fig. 10b focuses on the intensity of the peak associated to the C = C conjugation bond. The area corresponding to the film processed at 135 Pa (estimated for two zones due to the film heterogeneity) is lower than that relative to the sample at 75 Pa, which is coherent with the conductivity results.

As a conclusion of this part, depositing at higher pressure for the conditions tested is unfavorable for obtaining uniform films with higher electrical conductivity.

3.5. Influence of the deposition duration

The demonstrated stable evaporation of SbCl₅ and the resulting continuous PEDOT deposition allow investigating the effect of deposition time on the characteristics of the films. Four deposition times, 30, 60, 90 and 150 min, were studied for identical deposition conditions, namely total pressure 75 Pa, SbCl₅/EDOT ratio 0.18 and T_{sub} 50 °C. First, the influence of films thickness on their optical transmittance was investigated. PEDOT films were deposited on purpose on 24 × 24 mm² microscope cover glass substrates (Deckglaser 0101062). A small Si coupon (2 × 2 cm²), partially covered with Kapton was also positioned on the substrate holder in each experiment, in order to measure the thickness of the deposited film. The small size of the samples and the precision limit of the balance did not allow the determination of the mass of the films.

Fig. 11a presents the evolution of the film thickness and conductivity as a function of the deposition time. The thickness increases linearly from 13 nm at 30 min to 58 nm at 150 min, corresponding to a 0.4 nm/min constant deposition rate, showing the stability of the polymerization process.

All samples present similar electrical conductivity close to 700 S/cm, indicating that for the conditions tested, conductivity is not influenced by the film thickness between 13 and 58 nm. In addition, the evaporated masses of EDOT and SbCl₅ during each run (not shown) also linearly correlate with the total evaporation time for each compound, confirming the stability and reproducibility of the EDOT and oxidant evaporation rates.

Fig. 11b shows the optical transmittance (T%) of the films and their evolution as a function of the deposit duration, for the wavenumber range 300–800 nm, close to the visible one. Using an as received glass coupon as the reference, the 13 nm thick film deposited during 30 min presents a 96% transparency at 550 nm. This wavenumber is typically

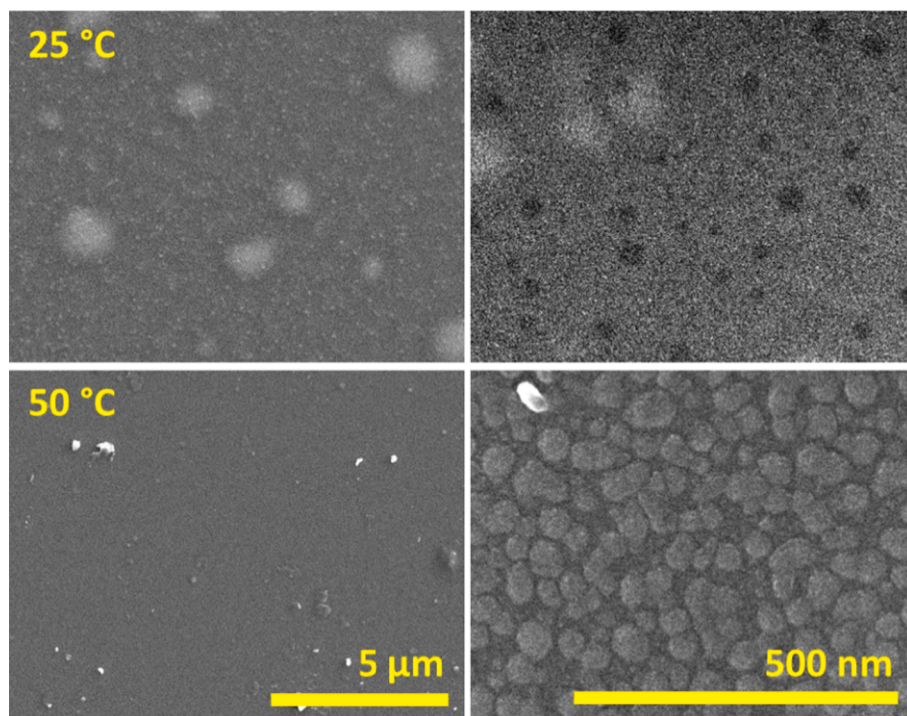


Fig. 8. FEG SEM views at two magnifications of films prepared at T_{sub} of 25 °C and 50 °C (total pressure of 75 Pa, $\text{SbCl}_5/\text{EDOT}$ ratio of 0.18 and deposition duration of 30 min).

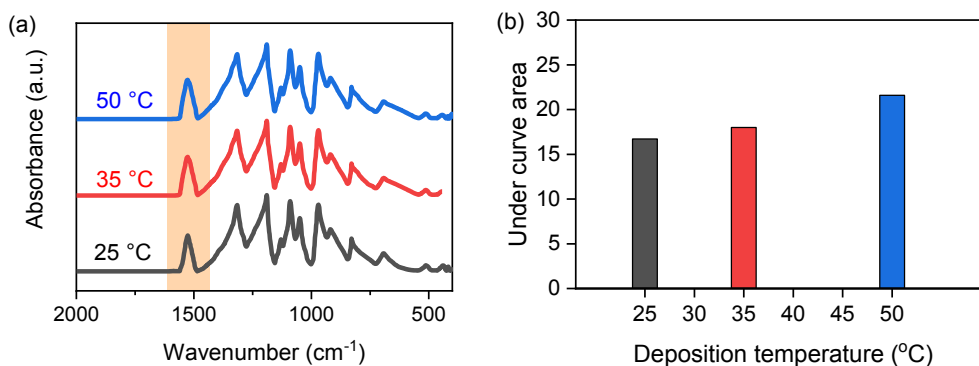


Fig. 9. PEDOT films deposited at T_{sub} of 25 °C, 35 °C and 50 °C. (a) FTIR spectra, (b) Evolution of the under curve area of the C = C stretching peak at 1527 cm^{-1} .

Table 1

Mass, deposition rate, thickness and electrical conductivity of PEDOT films deposited at two different total pressures of 75 and 135 Pa (T_{sub} of 50 °C, deposition duration of 30 min, $\text{SbCl}_5/\text{EDOT}$ ratio of 0.18).

Pressure (Pa)	Film mass (mg)	Deposition rate (mg/min)	Thickness (nm)	Conductivity (S/cm)
75	0.08 ± 0.04	0.003 ± 0.001	12 ± 4	770 ± 56
135	3.46 ± 0.05	0.115 ± 0.002	287 ± 267	537 ± 116

chosen as it represents the maximal intensity of sunlight in the region of green light [33] and the highest sensitive wavenumber to human eyes [34].

This value decreases slightly to 95% and 93% with increasing thickness. These results indicate that the optical characteristics of such oCVD PEDOT films are compatible with optoelectronic applications like OLEDs and solar cells which require transparent anodes [35]. The transmittance values are comparable with those of Gharahcheshmeh

et al. for PEDOT- SbCl_5 (97% for 10 nm) [25], PEDOT- VOCl_3 ($T = 93\%$ for 70 nm and 97% for 10 nm) [23] and slightly higher than PEDOT- FeCl_3 by Kovacik et al. ($T = 90\%$ for 27 nm) [36] and PEDOT- FeCl_3 by Lock et al. [8] ($T = 84\%$ for 35 nm).

Fig. 12 presents AFM maps of two films deposited on Si for 30 min and 90 min, on two areas, of $10 \times 10 \mu\text{m}^2$ and a $1 \times 1 \mu\text{m}^2$. Maps of the film surface after 30 min of deposition reveal the presence of a dense film with isolated, 40–50 nm high peaks. A similar morphology prevails on surfaces after 90 min deposition, however with an increasing peaks height, which reaches 90–100 nm. These islands probably do not correspond to the rich benzoid form particles in the bright zones of Fig. 5, since the film conductivity is unchanged, which could be due to the positive combination of the low EDOT/oxidant ratio, low total pressure and high T_{sub} used. Observations of smaller areas on the smoothest zones (Fig. 12c and 12d) indicate that the surface of the film deposited for 30 min is composed of a puzzle of beads whose lateral dimension is in the order of 50 nm. These beads are getting more faceted, larger and rougher with increasing the deposition time. The RMS roughness over the smooth surface parts increases from 4 nm at 30 min to 8 nm at 90 min. It is worth noting that this evolution of

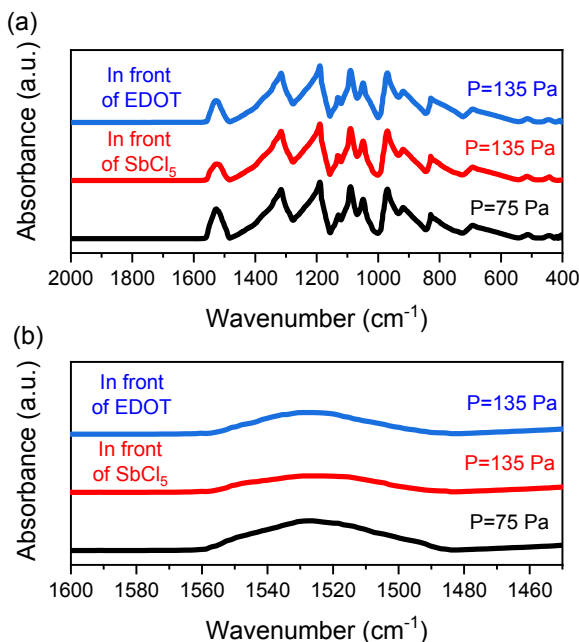


Fig. 10. (a) FTIR spectra of samples produced at 75 and 135 Pa, (b) Evolution of the C = C stretching peak (T_{sub} of 50 °C, deposition duration of 30 min, SbCl₅/EDOT ratio of 0.18).

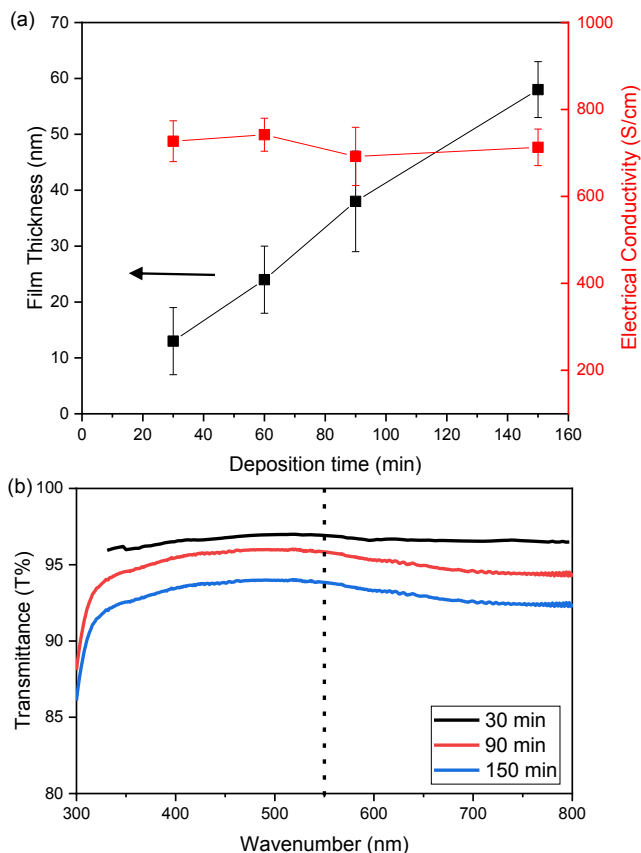


Fig. 11. Evolution of (a): film thickness and conductivity and (b): film UV-Vis transmittance as a function of deposition duration (T_{sub} of 50 °C, total pressure of 75 Pa, SbCl₅/EDOT ratio of 0.18).

morphology and roughness does not modify the electrical conductivity of the films.

3.6. Study of the uniformity at large scale

In a similar way as in our previous work on PEDOT-FeCl₃, an experiment was conducted involving ten $1 \times 1 \text{ cm}^2$ Si coupons fixed vertically on a scaffold structure into the reactor, with the aim to get insight into the PEDOT deposition mechanisms [11]. The coupons were placed over four levels of the scaffold at a 5 cm distance from each other, as schematized in Fig. 13. In addition, a Si wafer was also placed on the substrate holder. One third of each coupon was covered by Kapton for thickness measurements. The inlet molar SbCl₅/EDOT ratio was 0.18, T_{sub} was fixed at 25 °C and the run duration was 30 min. Two positions on each substrate were simultaneously probed for film thickness and conductivity.

The thickness values of all samples are reported in Fig. 13. It is shown that the deposition occurred uniformly on all ten positions within the reactor volume with a 52 nm average film thickness. A similar thickness was measured on the sample positioned at the top of the reactor, which is close to the one reported for the same deposition conditions in Section 3.2. The standard deviation is of 8% over the ten coupons. Similarly, the average electrical conductivity is close to 600 S/cm for all samples, as for the same deposition conditions of Section 3.2.

No solid residues were found in the reactor. This information combined with the result about the film thickness uniformity allows concluding that there are no gas phase reactions taking place during the deposition. As the diffusivity of the gas phase is high due to the prevailing low operating pressure, this result indicates that the oxidant and EDOT concentrations are identical at every point into the reactor. In the opposite case, the presence of gas phase reactions resulting in various gaseous intermediate species would have considerably reduced the precursors concentration along the scaffold height, leading to a decreasing deposition rate profile from the gas inlet to the reactor outlet. As a conclusion, over and above film uniformity, there are only surface reactions involved in the Step Growth Polymerization of PEDOT by SbCl₅, similarly to the oCVD process with FeCl₃ [11].

Finally, this scaffold experiment demonstrates that the developed oCVD process is fully reproducible and that PEDOT can be uniformly deposited on several tens of cm² substrates. The obtained results pave the way towards the scaling up of the PEDOT-SbCl₅ oCVD process over large surfaces.

4. Conclusions

SbCl₅ was investigated as oxidant for the production of PEDOT films, with the aim to develop a robust, full dry oCVD process. The stability over time of SbCl₅ evaporation was demonstrated by dedicated evaporation experiments, thus offering the possibility to control the oCVD process. Correlations between key process parameters (including inlet molar oxidant/EDOT ratio, substrate temperature, total pressure and deposition duration), film characteristics and properties were for the first time thoroughly studied.

The electrical conductivity of the films increased by decreasing the oxidant/EDOT ratio and by increasing the substrate temperature, as for the classical FeCl₃ oCVD oxidant. An opposite influence of the substrate temperature was observed on the deposited mass and thickness, which can be attributed to the significantly lower oxidant/EDOT ratios used with SbCl₅ compared to values reported in studies with FeCl₃, in addition to the higher volatility of the former. An increase of total pressure was detrimental to the film uniformity and conductivity, but increased considerably the deposition rate. The morphology of the film is clearly sensitive to the deposition conditions. In particular, the presence of poorly conductive benzoid PEDOT islands on the film can be highly reduced by optimizing the deposition parameters. The absence of post deposition liquid rinsing allowed developing a full dry process, opening

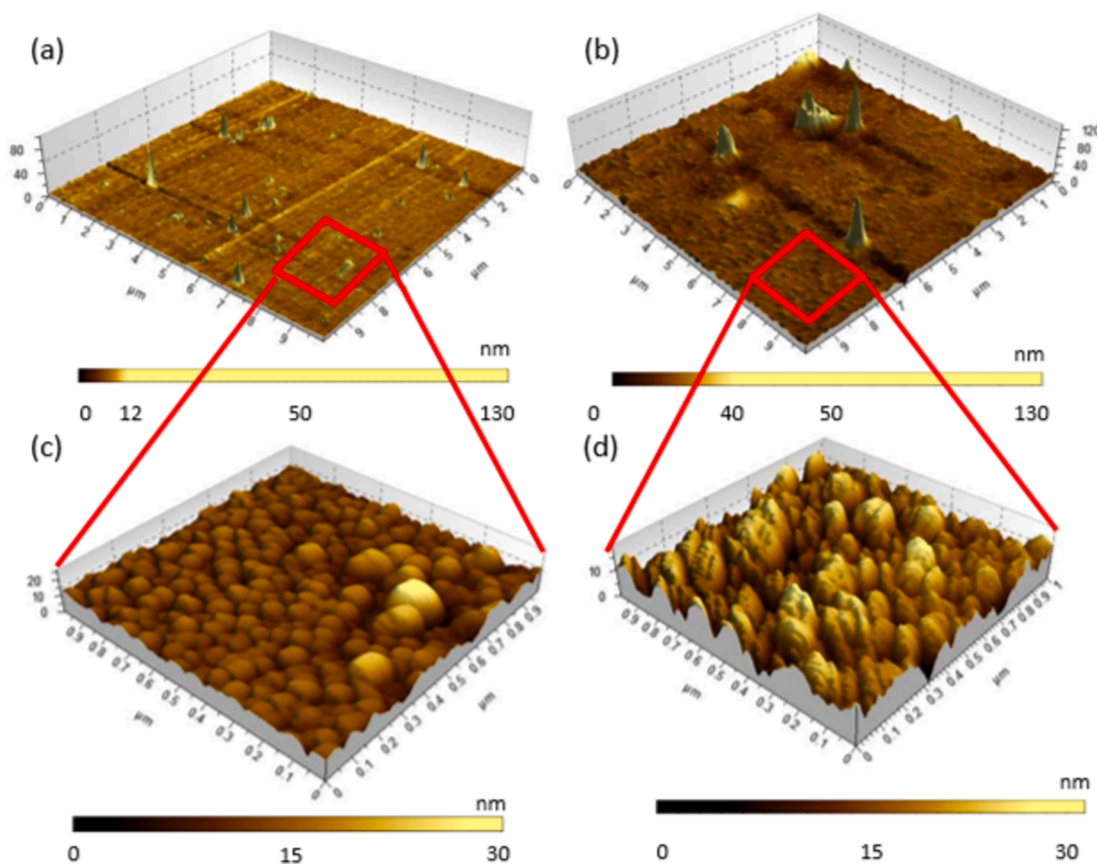


Fig. 12. AFM maps of two films deposited during 30 min (left) and 90 min (right). The upper and lower maps correspond to $10 \times 10 \mu\text{m}^2$ and $1 \times 1 \mu\text{m}^2$ areas, respectively (T_{sub} of 50°C , total pressure of 75 Pa, $\text{SbCl}_5/\text{EDOT}$ ratio of 0.18).

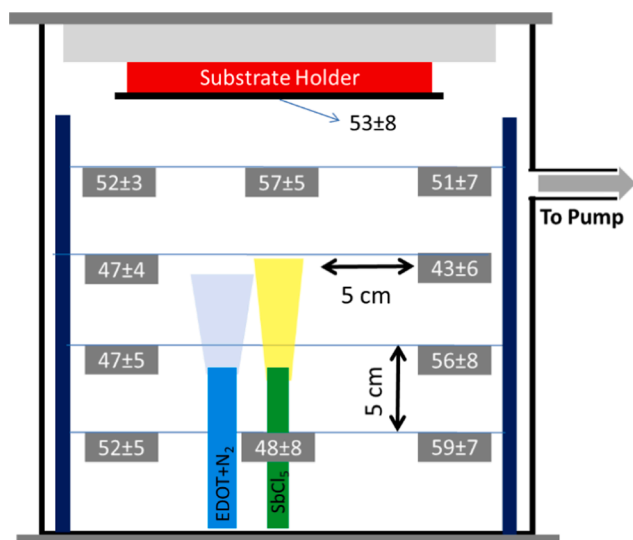


Fig. 13. Thickness values (in nm) over ten $1 \times 1 \text{ cm}^2$ Si coupons on a scaffold structure.

the way to the treatment of fragile substrates, like paper or fabrics.

Finally, the thickness uniformity of deposited films all over the oCVD reactor was proved for depositions at 75 Pa using a scaffold structure. This uniformity associated with the whole results obtained indicate that for the conditions tested, the process operates in the kinetically limited regime, with an overall polymerization kinetics limited by the SbCl_5 local concentration near the substrate.

This study demonstrates the reproducibility and the capability of this fully dry SbCl_5 oCVD process to be scaled up over larger surfaces. This opens the way to its industrial development in the fabrication of optoelectronic or sensing devices. It is worth noting that the absence of water in this oCVD process portends improved durability over time of the devices which could use PEDOT- SbCl_5 oCVD in substitution of the classical PEDOT:PSS route.

Declaration of Competing Interest

The authors declare that they have no known competing financial interests or personal relationships that could have appeared to influence the work reported in this paper.

Acknowledgments

We are indebted to C. Tendo and O. Marsan (CIRIMAT), C. Josse and T. Hungria (UMS Castaing), and M.L. de Solan Bethmale (LGC SAP) for their contribution concerning sample characterizations. We would like to thank J. Compain (LGC), D. Samelot, and D. Sadowski (CIRIMAT) for their help in preparing the experimental setup.

Appendix A. Supplementary material

Supplementary data to this article can be found online at <https://doi.org/10.1016/j.apsusc.2021.149501>.

References

- [1] M. Morales-Masis, S. De Wolf, R. Woods-Robinson, J.W. Ager, C. Ballif, Transparent electrodes for efficient optoelectronics, *Adv. Electron. Mater.* 3 (2017) 1600529, <https://doi.org/10.1002/aeml.201600529>.

- [2] X. Wang, X. Zhang, L. Sun, D. Lee, S. Lee, M. Wang, J. Zhao, Y. Shao-Horn, M. Dincă, and T. Palacios, High electrical conductivity and carrier mobility in oCVD PEDOT thin films by engineered crystallization and acid treatment, *Sci. Adv.*, 4 (2018) eaat5780.
- [3] M.H. Gharahcheshmeh, K.K. Gleason, Device fabrication based on oxidative chemical vapor deposition (oCVD) synthesis of conducting polymers and related conjugated organic materials, *Adv Mat Interfaces* 6 (2019) 1801564, <https://doi.org/10.1002/admi.201801564>.
- [4] L. Matějka, L. Merhari, *Hybrid nanocomposites for nanotechnology: electronic, optical, magnetic and biomedical applications*, Springer, Germany, 2009.
- [5] A. Elschner, S. Kirchmeyer, W. Lovenich, U. Merker, K. Reuter, *PEDOT: principles and applications of an intrinsically conductive polymer*, CRC Press, USA, 2010.
- [6] F. Zabihi, Y. Xie, S. Gao, M. Eslamian, Morphology, conductivity, and wetting characteristics of PEDOT: PSS thin films deposited by spin and spray coating, *Appl. Surf. Sci.* 338 (2015) 163–177, <https://doi.org/10.1016/j.apsusc.2015.02.128>.
- [7] J. Kim, E. Kim, Y. Won, H. Lee, K. Suh, The preparation and characteristics of conductive poly (3, 4-ethylenedioxythiophene) thin film by vapor-phase polymerization, *Synth. Met.* 139 (2003) 485–489, [https://doi.org/10.1016/S0379-6779\(03\)00202-9](https://doi.org/10.1016/S0379-6779(03)00202-9).
- [8] J.P. Lock, S.G. Im, K.K. Gleason, Oxidative chemical vapor deposition of electrically conducting poly (3, 4-ethylenedioxythiophene) films, *Macromolecules* 39 (2006) 5326–5329, <https://doi.org/10.1021/ma060113o>.
- [9] M.A. Ali, K.-H. Wu, J. McEwan, J. Lee, Translated structural morphology of conductive polymer nanofilms synthesized by vapor phase polymerization, *Synth. Met.* 244 (2018) 113–119, <https://doi.org/10.1016/j.synthmet.2018.07.007>.
- [10] S.G. Im, D. Kusters, W. Choi, S.H. Baxamusa, M. Van de Sanden, K.K. Gleason, Conformal coverage of poly (3, 4-ethylenedioxythiophene) films with tunable nanoporosity via oxidative chemical vapor deposition, *ACS Nano* 2 (2008) 1959–1967, <https://doi.org/10.1021/nn800380e>.
- [11] M. Mirabedin, H. Vergnes, N. Caussé, C. Vahlas, B. Caussat, An out of the box vision over oxidative chemical vapor deposition of PEDOT involving sublimed iron trichloride, *Synth. Met.* 266 (2020), 116419, <https://doi.org/10.1016/j.synthmet.2020.116419>.
- [12] M.C. Barr, C. Carbonera, R. Po, V. Bulović, K.K. Gleason, Cathode buffer layers based on vacuum and solution deposited poly (3, 4-ethylenedioxythiophene) for efficient inverted organic solar cells, *Appl. Phys. Lett.* 100 (2012) 97, <https://doi.org/10.1063/1.4709481>.
- [13] S.G. Im, K.K. Gleason, Systematic control of the electrical conductivity of poly (3, 4-ethylenedioxythiophene) via oxidative chemical vapor deposition, *Macromolecules* 40 (2007) 6552–6556, <https://doi.org/10.1021/ma0628477>.
- [14] S.G. Im, K.K. Gleason, E.A. Olivetti, Doping level and work function control in oxidative chemical vapor deposited poly (3, 4-ethylenedioxythiophene), *Appl. Phys. Lett.* 90 (2007), 152112, <https://doi.org/10.1063/1.2721376>.
- [15] S.P. Arnold, J.K. Harris, B. Neelamraju, M. Rudolph, E.L. Ratcliff, Microstructure-dependent electrochemical properties of chemical-vapor deposited poly (3, 4-ethylenedioxythiophene)(PEDOT) films, *Synth. Met.* 253 (2019) 26–33, <https://doi.org/10.1016/j.synthmet.2019.04.022>.
- [16] G. Drewelow, H.W. Song, Z.-T. Jiang, S. Lee, Factors controlling conductivity of PEDOT deposited using oxidative chemical vapor deposition, *Appl. Surf. Sci.* (2019), 144105, <https://doi.org/10.1016/j.apsusc.2019.144105>.
- [17] C. Vahlas, B. Caussat, W.L. Gladfelter, F. Senocq, E.J. Gladfelter, Liquid and solid precursor delivery systems in gas phase processes, *Recent Pat. Mater. Sci.* 8 (2015) 91–108, <https://doi.org/10.2174/1874464808666150324230711>.
- [18] R.M. Howden, E.D. McVay, K.K. Gleason, oCVD poly (3, 4-ethylenedioxythiophene) conductivity and lifetime enhancement via acid rinse dopant exchange, *J. Mater. Chem. A* 1 (2013) 1334–1340, <https://doi.org/10.1039/C2TA00321J>.
- [19] H. Chelawat, S. Vaddiraju, K. Gleason, Conformal, conducting poly (3, 4-ethylenedioxythiophene) thin films deposited using bromine as the oxidant in a completely dry oxidative chemical vapor deposition process, *Chem. Mater.* 22 (2010) 2864–2868, <https://doi.org/10.1021/cm100092c>.
- [20] D. Farka, A.O. Jones, R. Menon, N.S. Sariciftci, P. Stadler, Metallic conductivity beyond the Mott minimum in PEDOT: Sulphate at low temperatures, *Synth. Met.* 240 (2018) 59–66, <https://doi.org/10.1016/j.synthmet.2018.03.015>.
- [21] S.E. Atanasov, M.D. Losego, B. Gong, E. Sachet, J.P. Maria, P.S. Williams, G. N. Parsons, Highly conductive and conformal poly (3, 4-ethylenedioxythiophene) (PEDOT) thin films via oxidative molecular layer deposition, *Chem. Mater.* 26 (2014) 3471–3478, <https://doi.org/10.1021/cm500825b>.
- [22] G.L. Xu, Q. Liu, K.K.S. Lau, Y. Liu, X. Liu, H. Gao, X. Zhou, M. Zhuang, Y. Ren, J. Li, M. Shao, M. Ouyang, F. Pan, Z. Chen, K. Amine, G. Chen, Building ultraconformal protective layers on both secondary and primary particles of layered lithium transition metal oxide cathodes, *Nat Energy* 4 (2019) 484–494, <https://doi.org/10.1038/s41560-019-0387-1>.
- [23] M.H. Gharahcheshmeh, M.M. Tavakoli, E.F. Gleason, M.T. Robinson, J. Kong, and K.K. Gleason, Tuning, optimization, and perovskite solar cell device integration of ultrathin poly (3, 4-ethylene dioxothiophene) films via a single-step all-dry process, *Sci. Adv.*, 5 (2019) eaay0414, <https://doi.org/10.1126/sciadv.aay0414>.
- [24] S. Kaviani, M. Mohammadi Ghaleni, E. Tavakoli, S. Nejati, Electroactive and Conformal Coatings of oCVD Polymers for Oxygen Electroreduction, *ACS Appl. Polym. Mater.* (2019), <https://doi.org/10.1021/acsapm.8b00240>.
- [25] M.H. Gharahcheshmeh, M.T. Robinson, E.F. Gleason, K.K. Gleason, Optimizing the optoelectronic properties of face-on oriented poly(3,4-ethylenedioxythiophene) via water-assisted oxidative chemical vapor deposition, *Adv. Funct. Mater.* (2020) 2008712, <https://doi.org/10.1002/adfm.202008712>.
- [26] D.R. Stull, Vapor pressure of pure substances. *Organic and inorganic compounds*, *Ind. Eng. Chem.* 39 (1947) 517–540.
- [27] F. Smits, Measurements of sheet resistivities with the four point probe, *Bell system Techn. J.* 37 (1958) 711–718.
- [28] N. Cheng, T.L. Andrew, Reactive vapor deposition of conjugated polymer films on arbitrary substrates, *J. Visualized Exp.* (2018), e56775, <https://doi.org/10.3791/56775>.
- [29] K.K. Gleason, C.V.D. Polymers, *Fabrication of Organic Surfaces and Devices*, John Wiley & Sons, 2015.
- [30] X. Li, A. Rafie, V. Kalra, K.K.S. Lau, Deposition behavior of polyaniline on carbon nanofibers by oxidative chemical vapor deposition, *Langmuir* 36 (2020) 13079–13086, <https://doi.org/10.1021/acs.langmuir.0c02539>.
- [31] T.L. Andrew, L. Zhang, N. Cheng, M. Baima, J.J. Kim, L. Allison, S. Hoxie, Melding vapor-phase organic chemistry and textile manufacturing to produce wearable electronics, *Acc. Chem. Res.* 51 (2018) 850–859, <https://doi.org/10.1021/acs.accounts.7b00604>.
- [32] D. Bilger, S.Z. Homayounfar, T.L. Andrew, A critical review of reactive vapor deposition for conjugated polymer synthesis, *J. Mater. Chem. C* 7 (2019) 7159–7174, <https://doi.org/10.1039/C9TC01388A>.
- [33] A.S. Badday, A.Z. Abdullah, K.T. Lee, Application of heteropolyacid-based heterogeneous catalysts for conversion of oleochemicals into renewable fuels and other value-added products, *Mater. Sci. Forum* 757 (2013) 1–24, <https://doi.org/10.4028/www.scientific.net/MSF.757.1>.
- [34] J. Qiu, Y. Li, Y. Jia, *Persistent Phosphors: From Fundamentals to Applications*, Woodhead Publishing, 2020.
- [35] F. Gao, *Advanced nanomaterials for solar cells and light emitting diodes*, Elsevier, Netherlands, 2019.
- [36] P. Kovacic, G. del Hierro, W. Livernois, K.K. Gleason, Scale-up of oCVD: large-area conductive polymer thin films for next-generation electronics, *Mater. Horiz.* 2 (2015) 221–227, <https://doi.org/10.1039/C4MH00222A>.

Liquid antimony pentachloride as oxidant for robust oxidative chemical vapor deposition of Poly(3,4-ethylenedioxythiophene) films

Milad Mirabedin^{a, b}, Hugues Vergnes^a, Nicolas Causse^b,

Constantin Vahlas^b, Brigitte Caussat^{a*}

^a Laboratoire de Génie Chimique, Université de Toulouse, 4 allée Emile Monso, 31030 Toulouse cedex 4, France.

^b CIRIMAT, Université de Toulouse, 4 allée Emile Monso, 31030 Toulouse cedex 4, France.

EDX analyses of PEDOT simple with $\text{SbCl}_5/\text{EDOT}=0.42$

As shown in Figure S1, EDX analysis of these samples revealed presence of all PEDOT elements (C, S, ...) on the surface. Additionally, the film with $\text{SbCl}_5/\text{EDOT}=0.42$ was analyzed on a $\approx 5.5 \mu\text{m}$ line by EDX, across the dark background and the bright particles. We observe that all detected elements except Si show an increase in intensity when probing the particles. Fluctuations in Si intensity are associated with variable presence of other elements on the surface, attributed to the local increase in film thickness due to the presence of small particles. This evolution is confirmed when probing the large particle in the middle of the micrograph, with a significant increase in all components and a sharp decrease in Si intensity.

It is concluded that the PEDOT elements (C, S, O, Sb and Cl) are present everywhere on the film, as was the case for those deposited from FeCl_3 . Presence of all elements are higher on the big particle probably because of the smaller distance between the surface and the probe due to the height of these particles. The relative intensity of the probed particles remains qualitatively similar to the one of the background, in contrast to films deposited from FeCl_3 , which were locally richer in O and Fe. Such difference in composition of films deposited from the two

chemistries can be attributed to the fact that, in contrast to FeCl_3 , gaseous SbCl_5 cannot condensate in the adopted operating conditions. It can also be due to the lower oxidant/EDOT ratios used for the SbCl_5 experiments and to the fact that SbCl_5 is less moisture and air sensitive.

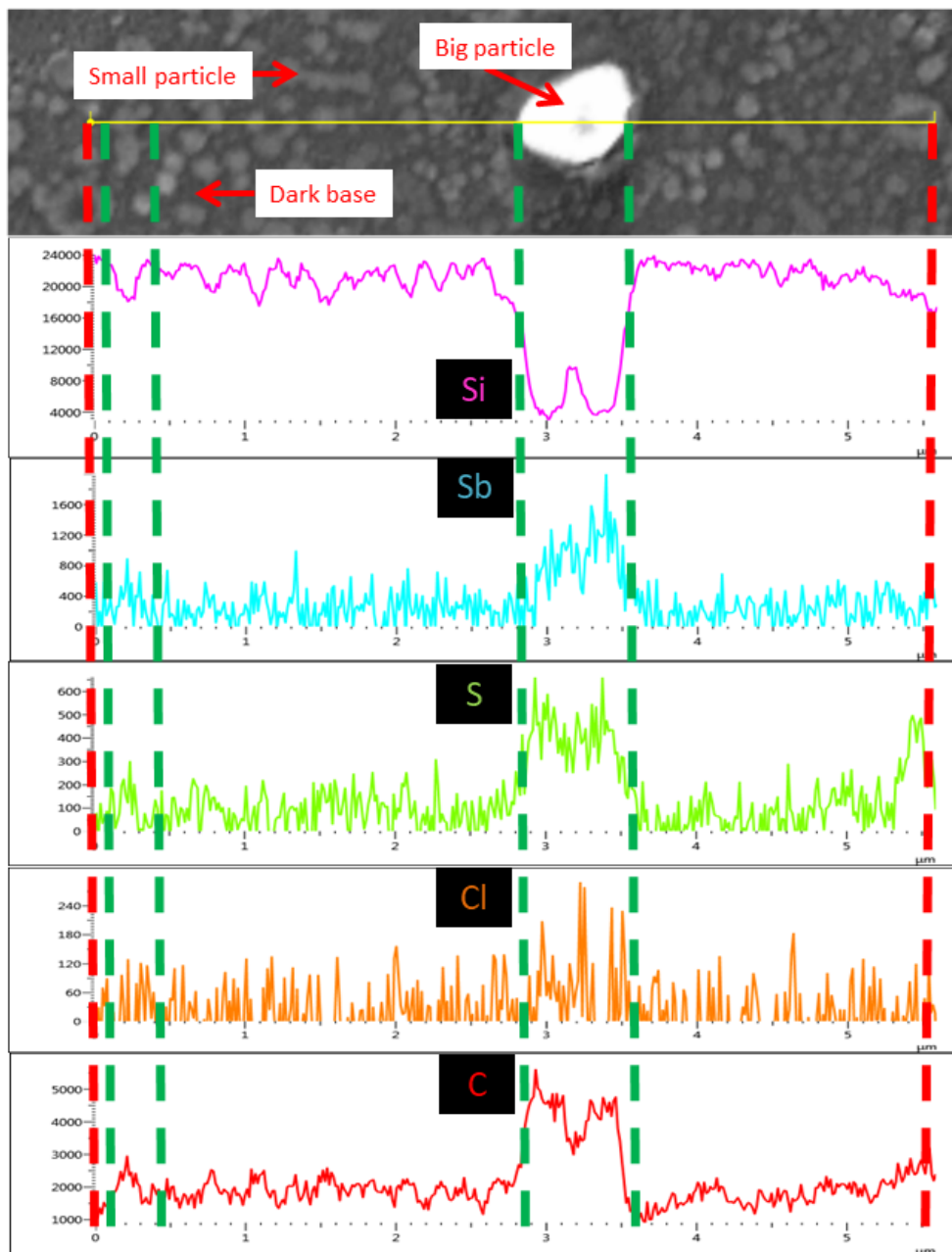


Figure S1. Linear EDX analysis across a 5.5 μm distance on sample with $\text{SbCl}_5/\text{EDOT}=0.42$.

The homogenous presence of Sb in EDX and independent XPS analyses suggest that some SbCl_5 might create Sb-complexes on the PEDOT film after losing two chlorine atoms through

polymerization and reduction. With this hypothesis, Sb remains trapped in the film forming links between SbCl_3 and the oxygen in monomer ethylenedioxy rings, as proposed by Kaviani et al. [1] for PEDOT films containing 2% mole Sb.

Raman analyses of the sample with $\text{SbCl}_5/\text{EDOT}=0.42$

The surface of the film with $\text{SbCl}_5/\text{EDOT}$ ratio 0.42 was locally analyzed by Raman spectrometry with the aim of identifying the possible differences between the large particles and the two other zones on the surface. Raman laser beam can analyze a smaller zone of the surface (probe size 700 nm) in comparison with the 1 cm probed area by FTIR. Considering the 700 nm diameter limit, we carefully chose these 3 areas to investigate their chemical composition. These zones correspond to large particles (Zone 1), small particles (Zone 2) and the dark base (Zone 3) in Figure S2.

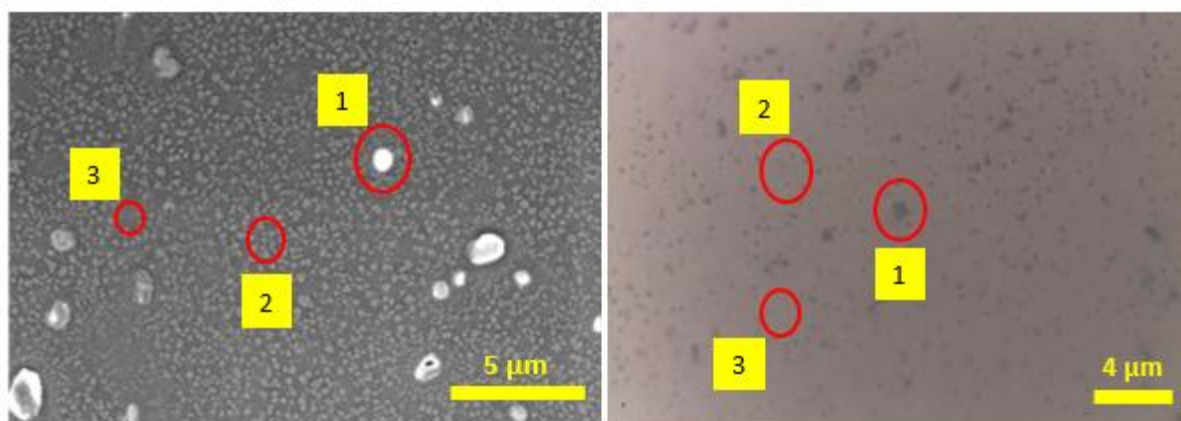


Figure S2. Visualization of three zones on sample with $\text{SbCl}_5/\text{EDOT}=0.42$ in SEM (left) and optical microscope (right) surface micrographs for Raman analysis.

Raman intensity of the small particles (zone 2) and of the background (zone 3) in the SEM micrograph indicates similar positions for all peaks, confirming the presence of PEDOT in the small particles (Figure S3). The intensity of all PEDOT peaks is systematically stronger on large particles (zone 1), attributed to the higher thickness of the film on this zone. This is why

the oxyethylene ring deformation peak at 990 cm^{-1} , which is seen on the large particles in zone 1 is covered by the silicon peak on other zones.

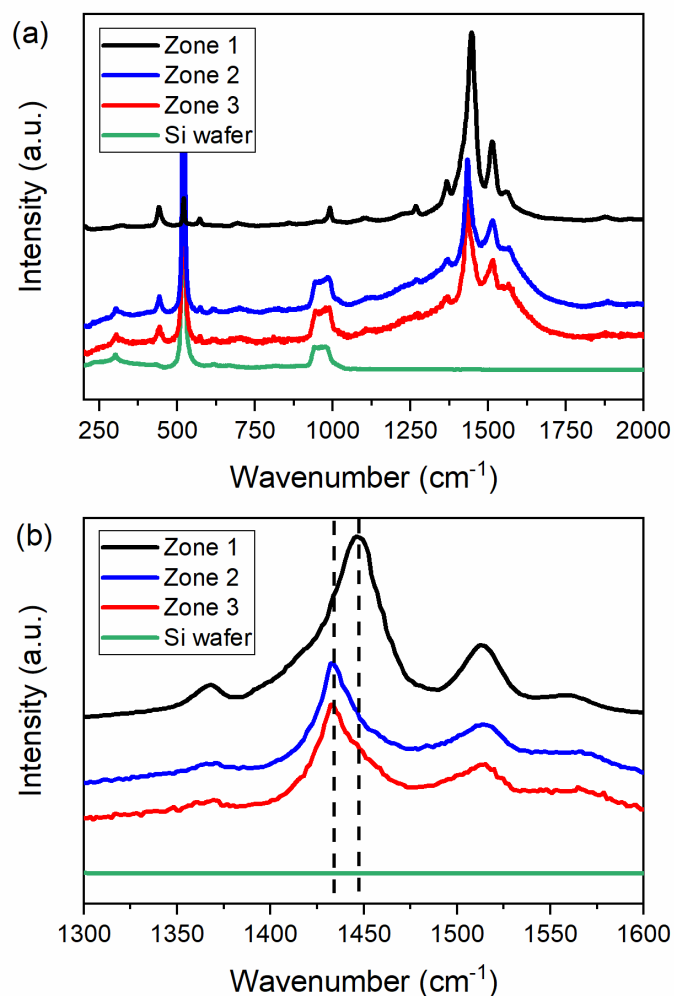


Figure S3. Raman spectra of sample with $\text{SbCl}_5/\text{EDOT}=0.42$ on three different zones.

A significant difference to note is the shift of the $\text{C}_\alpha=\text{C}_\beta$ symmetric peak in Table S1, from 1434 cm^{-1} to 1447 cm^{-1} on all large particles of zone 1, in comparison with the other zones. We attribute this shift to the non-uniform presence of quinoid (doped) and benzoid (undoped) PEDOT in the film, as is reported in [1, 2]. It appears that zone 1 is poorer in quinoid (doped) PEDOT in comparison with the other zones and consequently less conductive.

Table S1. Comparison of assigned peaks observed in the Raman of sample with SbCl₅/EDOT=0.42 with literature. Values in cm⁻¹.

Attribution	Tran-Van et al. [3]	Kaviani et al.	Zone 1	Zone 2	Zone 3
	with FeCl ₃	[1] with SbCl ₅			
C-O-C symmetric deformation	440	-	440	440	440
	-	857	861	860	860
	-	1092	1098	1099	1100
C-S-C symmetric deformation	-	693	693	693	693
Oxyethylene ring deformation	572	573	572	572	572
	988	990	990	Silicon	Silicon
C_α-C_α inter-ring stretching	1267	1262	1266	1266	1266
C_β-C_β stretching	1370	1363	1370	1370	1370
C_α=C_β symmetric stretching	1444	1430	1447	1434	1434
C_α=C_β antisymmetric stretching	1516	1512	1512	1513	1512

Let us note that this shift does not appear in the most conductive film with SbCl₅/EDOT=0.18. The Raman spectra of the sample deposited with the higher SbCl₅/EDOT ratio of 0.76, show that the C_α=C_β symmetric peak is present at 1447 cm⁻¹. No peak shift is observed between big and small particles on this sample. All peaks are similar to the peak at zone 1 on sample with ratio =0.42 with less quinoid PEDOT. In samples with less SbCl₅/EDOT ratio, we see a difference in the position of C_α=C_β symmetric peak for different zones. Zone 1 with large particles is shifted to right so has less doped PEDOT. As the ratio increases, although again these three zones are observed, there is less difference between quinoid and benzoid C_α=C_β symmetric peak positions as they both tend to shift to the benzoid form (shift to right). This means that these films with higher ratios have more undoped PEDOT. We see then a correlation between the position of C_α=C_β symmetric peak and the electrical conductivity as a function of the SbCl₅/EDOT ratio.

XPS results of a PEDOT-SbCl₅ film prepared under SbCl₅/EDOT=0.18

Figure S4 presents the high resolution XPS spectra of a PEDOT-SbCl₅ film prepared under SbCl₅/EDOT=0.18 and $T_{\text{sub}}=25^{\circ}\text{C}$. Table S2 presents the corresponding XPS elemental analysis. Sb was probed at an average concentration not exceeding 5 at.%, in agreement with the EDX results.

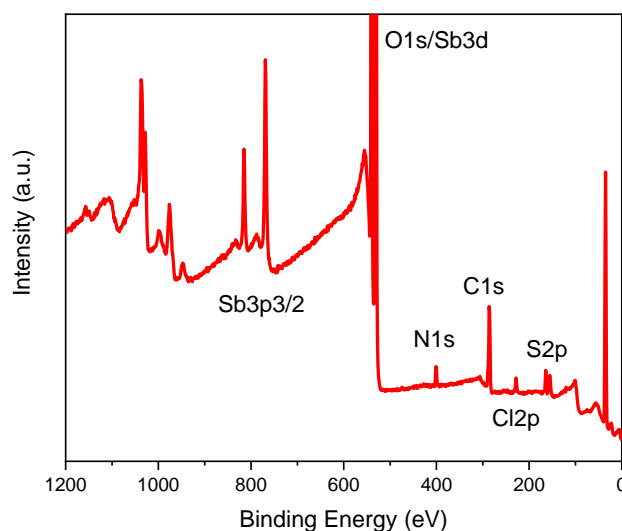


Figure S4. (a) XPS core-level survey of PEDOT-SbCl₅ via oCVD at SbCl₅/EDOT=0.18 and $T_{\text{sub}}=25^{\circ}\text{C}$.

Table S2. XPS elemental analysis of as-deposited PEDOT-SbCl₅ film at SbCl₅/EDOT=0.18 and $T_{\text{sub}}=25^{\circ}\text{C}$.

Name	Peak BE (eV)	FWHM (eV)	Atomic %
Sb4d	35.27	2.36	0.00
S2p cycle	163.89	1.03	3.58
S2p cycle	165.11	1.09	1.79
S2p	168.25	1.76	0.34
S2p	169.40	2.16	0.17
Cl2p	200.71	0.89	0.47
C1s CC, CH	284.84	1.36	17.28
C1s C-O, CS	286.35	1.55	24.72
C1s C=O	287.93	1.83	4.61
C1s O=C-O	289.00	1.83	3.74
N1s	400.43	3.14	1.43
Sb3d5/2	530.97	1.46	2.78
O1s C=O, other	531.41	1.30	19.05
O1s C-O	533.10	1.54	18.46
Sb3d3/2	540.40	1.44	1.58
Sb3p3/2	769.02	3.66	0.00

FTIR analyses of samples with SbCl₅/EDOT ratios from 0.18 to 2.08 (T_{sub}=25°C)

Table S3 presents the assigned peaks of PEDOT films at ambient temperature and different SbCl₅/EDOT ratios.

Table S3. Comparison of assigned FTIR frequencies for present samples and the reference

Vibration mode	Present samples	Kaviani et al. (2019)
C-O-C deformation	440	434
	518	520
C-S-C stretching	696	685
	827	825
	919	921
	971	970
C-O-C stretching	1048	1048
	1091	1085
	1127	1135
	1189	1187
C-C intra-ring	1319	1309
C=C antisymmetric stretching	1527	1515

Effect of substrate temperature on film thickness uniformity

Figure S5 shows the thickness uniformity of PEDOT films prepared at three substrate temperatures of 25, 35 and 50°C and the SbCl₅/EDOT=0.18. No evolution of thickness uniformity by depositing at higher substrate temperatures was observed.

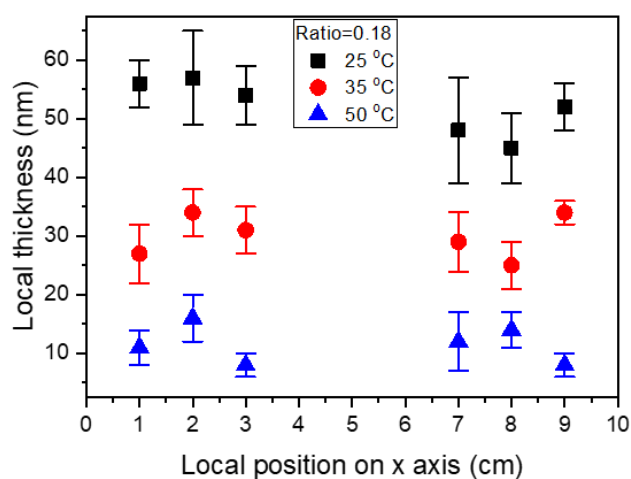


Figure S5. Thickness profile over Si wafer for depositions at T_{sub}=25, 35 and 50°C and SbCl₅/EDOT=0.18.

Raman analysis of the sample with $\text{SbCl}_5/\text{EDOT}=0.18$ and $T_{\text{sub}}=50^\circ\text{C}$

The Raman spectra are shown in Figure S6 for bright particles and small particles seen on the surface in Figure 8. These results are significantly different from those in Figure S3 as the bright particles on the surface show the $\text{C}\alpha=\text{C}\beta$ symmetric peak in the same position as the small particles, both at 1435 cm^{-1} . Again, observation of the peak at this wavenumber shows more quinoid (doped) PEDOT in the film, by increasing the substrate temperature [1, 2].

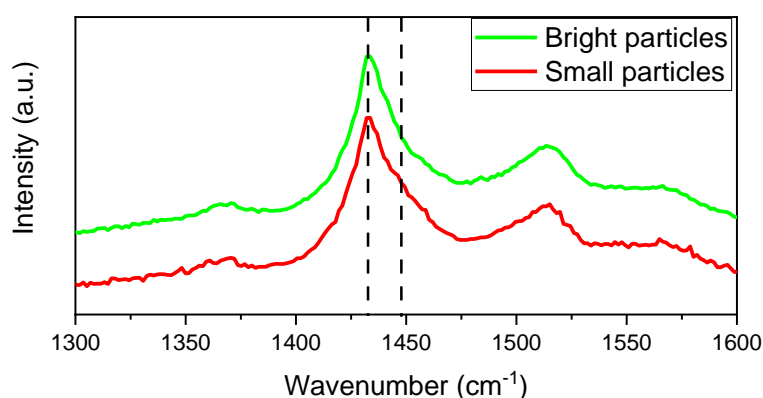


Figure S6. Raman spectra of sample with $\text{SbCl}_5/\text{EDOT}=0.18$ at $T_{\text{sub}}=50^\circ\text{C}$ on the bright and particles in Figure 8.

XRD analysis of the sample with $\text{SbCl}_5/\text{EDOT}=0.18$ and $T_{\text{sub}}=50^\circ\text{C}$.

Figure S7 presents the XRD spectrum. The absence of any peak suggests amorphous structure of the polymer, similar to the observations of Kaviani et al. [1].

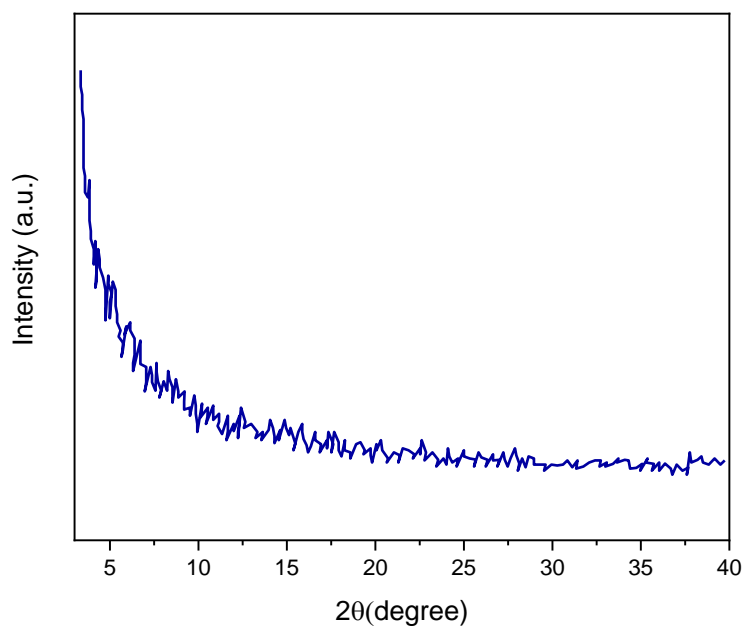


Figure S7. XRD analysis of the sample with $\text{SbCl}_5/\text{EDOT}=0.18$ prepared at $T_{\text{sub}}=50^\circ\text{C}$.

Effect of total pressure on film thickness uniformity

Figure S8 shows the thickness measurements on the surface of the Si wafer for two different deposition pressures of 75 and 135 Pa. The uniformity is improved at lower pressure.

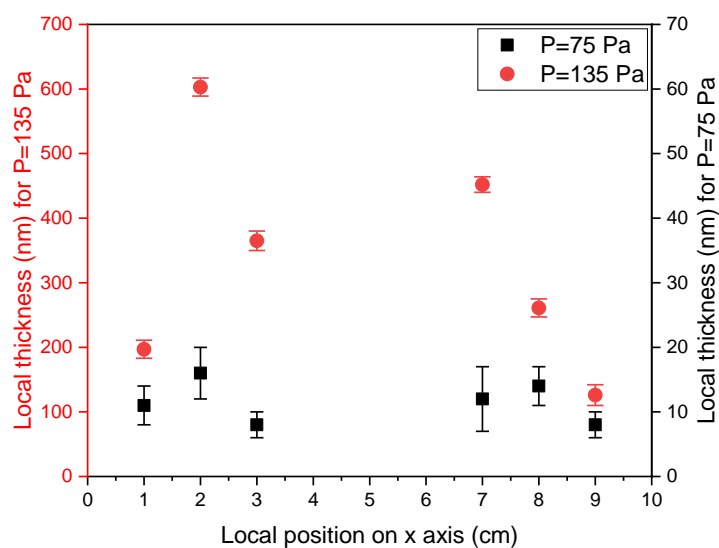


Figure S8. Thickness profile over the silicon wafer for two different total pressures of 75 and 135 Pa.

References

1. Kaviani, S., et al., Electroactive and Conformal Coatings of oCVD Polymers for Oxygen Electroreduction, ACS Appl. Polym. Mater., (2019) <https://doi.org/10.1021/acsapm.8b00240>.
2. Pistillo, B., et al., One step deposition of PEDOT films by plasma radicals assisted polymerization via chemical vapour deposition, J. Mater. Chem. C, 4 (2016) 5617-5625. <https://doi.org/10.1039/C6TC00181E>
3. Tran-Van, F., et al., Fully undoped and soluble oligo (3, 4-ethylenedioxythiophene) s: spectroscopic study and electrochemical characterization, J. Mater. Chem., 11 (2001) 1378-1382. <https://doi.org/10.1039/B100033K>.